

We are IntechOpen, the world's leading publisher of Open Access books Built by scientists, for scientists

4,800

Open access books available

122,000

International authors and editors

135M

Downloads

Our authors are among the

154

Countries delivered to

TOP 1%

most cited scientists

12.2%

Contributors from top 500 universities



WEB OF SCIENCE™

Selection of our books indexed in the Book Citation Index
in Web of Science™ Core Collection (BKCI)

Interested in publishing with us?
Contact book.department@intechopen.com

Numbers displayed above are based on latest data collected.

For more information visit www.intechopen.com



Chapter

Application of Fourier Analysis of Cerebral Glucose Metabolism in Color-Induced Long-Term Potentiation: A Novel Functional PET Spectroscopy (*f*PETS) Study in Mice

Philip C. Njemanze, Mathias Kranz and Peter Brust

Abstract

Fourier time-series analysis could be used to segregate changes in the ventral and dorsal streams of the visual system in male and female mice. Color memory processes of long-term potentiation and long-term depression could be identified through spectral analysis. We used small animal positron emission tomography and magnetic resonance imaging (PET/MRI) to measure the accumulation of [¹⁸F] fluorodeoxyglucose ([¹⁸F]FDG) in the mouse brain during light stimulation with blue and yellow filters compared to darkness condition. The mean standardized uptake values (SUV) of [¹⁸F]FDG for each stimulus condition was analyzed using standard Fourier analysis software to derive spectral density estimates for each condition. Spectral peaks were identified as originating from the subcortical region (S-peak) by subcortical long-term potentiation (SLTP) or depression (SLTD), and originating from the cortical region (C-peak) by cortical long-term potentiation (CLTP) or depression (CLTD). Luminance opponency occurred at S-peak by SLTP in the dorsal stream in the left visual cortex in male mice. On the other hand, chromatic opponency occurred by wavelength-differencing at C-peak by CLTP in the cortico-subcortical pathways in the ventral stream in the left visual cortex in male mice. In contrast in female mice, during luminance processing, there was resonance phenomenon at C-peak in the ventral stream in the right visual cortex. Chromatic opponency occurred at S-peak by SLTP in the dorsal stream in the right visual cortex in female mice. Application of Fourier analysis improved spatial and temporal resolutions of conventional *f*PET/MRI methods. Computation of color processing as a conscious experience has wide range applications in neuroscience and artificial intelligence.

Keywords: chromatic opponency, brain, light stimulation, sex, asymmetry, spectroscopy, memory

1. Introduction

Humans could discern as many as 10 million colors within the visible spectrum between 380 and 740 nm under normal conditions. Color processing is a memory computation within specific areas in the visual cortex. Conventionally, the visual system is segregated into the primary and secondary visual cortex. The primary visual cortex is organized into a ventral occipitotemporal stream for representation of “what” system, while the dorsal occipitoparietal stream demonstrates the “where” [1, 2]. The ventral stream implements hierarchical processing for object recognition, while the dorsal stream uses same for complex computation for motion in three-dimensional space. However, there is integration of information from both ventral and dorsal streams [3]. We applied conventional functional positron emission tomography and magnetic resonance imaging (*f*PET/MRI) technique to demonstrate gender-related cerebral metabolic changes during color processing in a mouse model [4]. The latter conventional approach could not segregate processes in the ventral and dorsal streams, respectively. We employed the use of conventional methods of animal PET/MR imaging [5] before we explored the use of Fourier analysis of the time series of the surrogate marker of cerebral metabolism of glucose during color processing.

The two visual streams are segregated in their arterial networks for blood flow supply in the visual cortex. The blood flow from the territories of the posterior (PCA) and middle (MCA) cerebral arteries [6] supply the visual pathways and extrastriate cortex “color centers” [5]. Color processing takes place within cortico-subcortical circuits working through the basal ganglia via the ventromedial occipital region to the posterior inferior temporal cortex, the latter is located along the anterior third of the calcarine sulcus [7]. The arteries of the circle of Willis segregate into two independent arterial systems called the cortical and ganglionic arteries, which do not communicate in any region of their peripheral distribution. Both systems are separated by a borderline of diminished nutritive activity [6].

The three primary qualities of color are hue, saturation (chroma), and lightness (value), and humans can differentiate over 10 million colors. Color vision implicates two main memory processes of simultaneous color contrast and color constancy [8–13]. The phenomenon that surround colors profoundly influence the perceived color has been attributed to simultaneous color contrast [9]. It is presumed that, simultaneous color contrast involves having a chromatic contrast detector subserving one area of the chromatic space, excite a chromatic detector of opposite type, and/or inhibit a chromatic detector of the same type in neighboring areas of chromatic space [8]. The mechanism for simultaneous color contrast may involve wavelength-differencing [13]. In human studies indexed using transcranial Doppler measured mean cerebral blood flow velocity (mCBFV) demonstrated selective response to colors of different wavelengths [14]. The application of Fourier time-series analysis of mCBFV described as functional transcranial Doppler spectroscopy (*f*TCDS) was used to demonstrate changes related to color processing [15–17] and facial processing [18, 19] in humans. Fourier analysis was applied to segregate the changes in the ventral and dorsal streams in the visual cortex [20].

There is need to develop reliable indices to characterize cellular processes occurring in specific regions in the visual cortex. Conventional imaging techniques do not provide specific indices with prerequisite resolution. However, PET images rendered in units of standardized uptake values (SUV) of [¹⁸F]FDG can be subjected to simple semi-quantitative analysis in animal models. Blood flow and metabolism, therefore, have been considered virtually equivalent, indirect indices of brain function [21]. Even though, some have demonstrated that there is regional uncoupling of CBF and CMRO₂, during neuronal activation induced by

somatosensory stimulation [22]. Conversely, rCBF has been found to correlate with mCBFV [23]. Brain neuronal activity, blood flow, and metabolism share common characteristics in the frequency domain, hence methods that uncover the spectral behavior of such systems could provide useful insight. It has been established that, there is a rationale for application of Fourier analysis to characterize the periodicity of biological systems and in particular the cerebrovascular system [24–26]. The presumption is that the vessels of the cortical arterial system are not so strictly “terminal” as those of the ganglionic system, and perfuse areas that could be mapped to retinotopic structures in the mouse visual cortex [27]. Therefore, the application of Fourier analysis could separate the frequency peaks from the cortical branches of the “ventral stream” from that of the ganglionic branches of the subcortical “dorsal stream.” In prior human studies indexed by f^{TCDS} , we differentiated processes in the cortical branches of the “ventral stream” at C-peak, from processes in the subcortical “dorsal stream” at S-peak [15, 16, 19]. The latter enabled us to localize brain function associated with the cortical (C-peak) processes within the ventral stream and differentiate them from subcortical (S-peak) processes within the dorsal stream of the visual cortex, in men and women, respectively.

Color is a brain computational process that involves memory. The color memory formation implicated known models of synaptic and cellular events [28, 29]. We propose to test the hypothesis that, Fourier time-series analysis of mean SUV values as surrogate marker of cerebral metabolism could uncover the underlying memory mechanisms associated with the phenomena of long-term potentiation (LTP) [28] and long-term depression (LTD) [29]. The effects of color stimulation are induced by the physical characteristics of light stimulus. Light has a dual nature of wave and particle, which conditions wavelength-differencing and frequency-differencing processes [15–17, 20] in the brain. The LUMINANCE effect responsiveness was demonstrated by comparing Dark versus Light conditions. The luminance axis is orthogonal (opposite) in direction to that of the chromatic axis. When the effects of longer wavelength color (Yellow) were accentuated over shorter wavelength color (Blue), it was presumed that WAVELENGTH-encoding is present [15]. On the other hand, when the effects of higher frequency color (Blue) were accentuated over lower frequency color (Yellow), ENERGY-encoding is present [15]. The occurrence of WAVELENGTH-encoding main effect at S-peaks, and at least a tendency for ENERGY-encoding at C-peaks results in WAVELENGTH-differencing [15]. WAVELENGTH-differencing could be accomplished [15], when a chromatic contrast detector in one area of chromatic space, activates a chromatic detector of opposite type, or on the other hand inhibits a chromatic contrast detector of similar function in adjoining areas of chromatic space [11]. FREQUENCY-differencing implements ENERGY-encoding main effect which accentuates C-peaks by cortical long-term potentiation (CLTP) process, and at least a tendency at S-peaks due to attenuation by subcortical long-term depression (SLTD). The converse processes are also feasible by subcortical long-term potentiation (SLTP) accentuating S-peaks and cortical long-term depression (CLTD) attenuating C-peaks.

The results in human studies demonstrated gender differences in mechanism of color memory processing indexed as processes analogous to long-term potentiation (LTP) [28] and long-term depression (LTD) [29]. In men, there was wavelength-differencing by CLTD and CLTP in the right hemisphere [16, 17], synchronously in the contralateral left hemisphere, there is cortical short-term depression (CSTD) and subcortical short-term potentiation (SSTP), coupled to exponential increase in synaptic strength, which may implicate NMDA receptors [16, 17, 28, 29], and thereafter, decays to asymptotic level. It was postulated that in men, in the contralateral left hemisphere, memory activation implicated “exponential expansion” by CSTD and SSTP processes. Conversely, in women, the processes of CLTP and SLTD

conditioned frequency-differencing within the left hemisphere [16, 17, 30]. Simultaneously, in the ipsilateral selective area in the left hemisphere, there was cortical short-term potentiation (CSTP) and subcortical short-term depression (SSTD) [11, 12, 17]. This was followed by logarithmic decay in synaptic strength to asymptotic levels, that maybe related to action of NMDA receptors. In contrast to that seen in men, in women, there was ipsilateral left hemisphere memory activation involving “logarithmic compression” by CSTP and SSTD processes. Analogous synaptic and cellular activities with opposite hemispheric localization have been observed in animal experiments [30, 31].

The origin of the C-peak and S-peak was demonstrated in human studies investigated using functional transcranial Doppler spectroscopy (f TCDS). The peaks were presumed to originate from peripheral reflection sites such as the tip of the fingers, the terminal end of the lenticulostriate subcortical arteries, and the terminal end of the cortical branches of the MCA. The peaks were designated as F-(fundamental), C-(cortical), and S-(subcortical) peaks and occurred at regular frequency intervals of 0.125, 0.25, and 0.375, respectively. If we assume that the fundamental frequency of cardiac oscillation is the mean heart rate, then these frequencies could be converted to cycles per second (Hz). The fundamental frequency f of the first harmonic is the mean heart rate per second, given by 74 bpm/60 seconds or 1.23 Hz in a normal person [18]. Therefore, the F-, C-, and S-peaks occurred at multiples of the first harmonic, at second and third harmonics, respectively. The calculated arterial lengths approximate visible arterial length of the lenticulostriate vessels from the main stem of the MCA on carotid angiograms [32]. Others have suggested that the estimated distances may not correlate exactly with known morphometric dimensions of the arterial tree [33].

We postulate that, the Fourier time-series analysis of the frequency-domain of cerebral metabolism may uncover the underlying memory mechanisms explained by LTP and [28] LTD [29], primarily because the models have properties expected of a synaptic associative memory mechanism, such as rapid induction, associative interactions, persistence, synapse specificity, and dependence on correlated synaptic activity. LTP and LTD remain only models of the synaptic and cellular events that may underlie memory formation.

The physical characteristics of light stimulus relate to its dual nature as a wave and particle. Light has the physical properties of amplitude, phase difference, wavelength, frequency, and resonance phenomenon. The mechanistic strategies for processing the physical properties of light could be separated into five categories: (a) variations in peak amplitude associated with excitatory processes of CLTP that result in accentuation of C-peak or SLTP that cause accentuation of S-peak from baseline [15–20]. Conversely, the change in peak amplitude maybe induced by inhibitory processes of CLTD resulting in attenuation of C-peak below baseline condition or SLTD causing attenuation of S-peak below baseline condition [15–20]. The patterns of activation could be in the right hemisphere (-R) or left hemisphere (-L). When changes in the cortical C-peak amplitudes are higher than that in the subcortical region, it was designated as cortico-subcortical activation pattern originating in the ventral stream. Conversely, when higher changes in amplitude occur for subcortical S-peak, it was designated as subcortico-cortical activation pattern originating in the dorsal stream. (b) Phase difference could be precluded if the oscillator generates a periodic signal and the phase detector compares the phase of that signal with the phase of the input periodic signal, adjusting the oscillator to keep the phases matched. The matched phases by mutual phase locking would mean keeping the same frequency as observed in neurons [34], otherwise frequency entrainment of the two oscillators. The latter is the basis of neuronal entrainment which refers to the capacity for natural synchronization of brain wave frequency

with the rhythm of periodic external stimuli, which could be visual, auditory, or tactile. The cortical (C-peak) and subcortical (S-peak) peaks are a result of the brain phase-locked loop which generates harmonic frequencies at multiples of the fundamental frequency [15–20], which is dependent on the heart rate. (c) Wavelength-differencing is a mechanism of chromatic opponency that separates the effects of longer wavelength color yellow from that of shorter wavelength color blue [15–20]. (d) Frequency-differencing is a mechanism of chromatic opponency that selectively detects colors of high-frequency color such as blue distinct from low-frequency colors such as yellow [15–20]. (e) Resonance is the ability of neurons to respond selectively to input at preferred frequencies [34]. The frequency oscillations that result to resonance could cause a synchronization phenomenon by adjustment of the rhythms of self-sustained periodic oscillations [34]. Luminance opponency is the difference between the effects of white light stimulation compared to the “color dark” light-absent condition. Spatial opponency was determined by significant differences between C-peak and S-peak for the same color such as the “color dark” otherwise expressed as value/lightness of colors. Within the three-dimensional color space, color and luminance interact at orthogonal planes [17].

Color is one aspect of an object, and another is the form, and the puzzle is on how it all comes together in the human perception of the object, which is commonly referred to as the “binding problem.” New techniques are required to investigate the binding problem which presents as a major challenge to cognitive neuroscientists and philosophers over several millennia. The first aspect of the problem (problem 1) is the segregation problem which attempts to understand the mechanistic strategies the brain employs to segregate elements in complex patterns of sensory inputs so that they are allocated to “discrete objects.” In other words a blue cube and a yellow disc are perceived as they are and not vice versa. The second aspect of the problem (problem 2) is the brain combinatorial computation employed to synthesize a holistic conscious experience [35, 36]. Both the binding problems 1 and 2 are inter-related and would require mechanistic strategies in both spatial and temporal dimensions. We postulate that problems 1 and 2 are resolved by combination of responses involving processes of cortical and subcortical long-term potentiation and depression (CLTP, CLTD, SLTP, and SLTD), within the ventral and dorsal streams in the visual cortex. Furthermore, other brain areas become implicated by synchronization within the same hemisphere or through trans-callosal connections to the contralateral hemisphere. There may be gender differences in cerebral asymmetry for color processing [15–20].

We aim to demonstrate the implementation of the mechanistic strategies for brain function in color processing using Fourier analysis of the time series of the SUV as a surrogate marker of cerebral metabolism of glucose. We hope that this new approach would be useful to resolve the binding problem of conscious experience. The latter approach we suggest to be called functional positron emission tomography spectroscopy (f PETS), analogous to f TCDS we already described elsewhere [15–19].

2. Methodological procedures

2.1 Mice

The experimental setup (**Figure 1**) has been described in detail elsewhere [5]. Briefly, five male and five female CD-1 mice (70–84 days old, 22–28 g) were housed in a vented temperature-controlled animal cabinet (HPP108, MEMMERT GmbH & Co. KG; Germany) under a 12 hour: 12 hour light:dark cycle (lights on at 7:00 am)

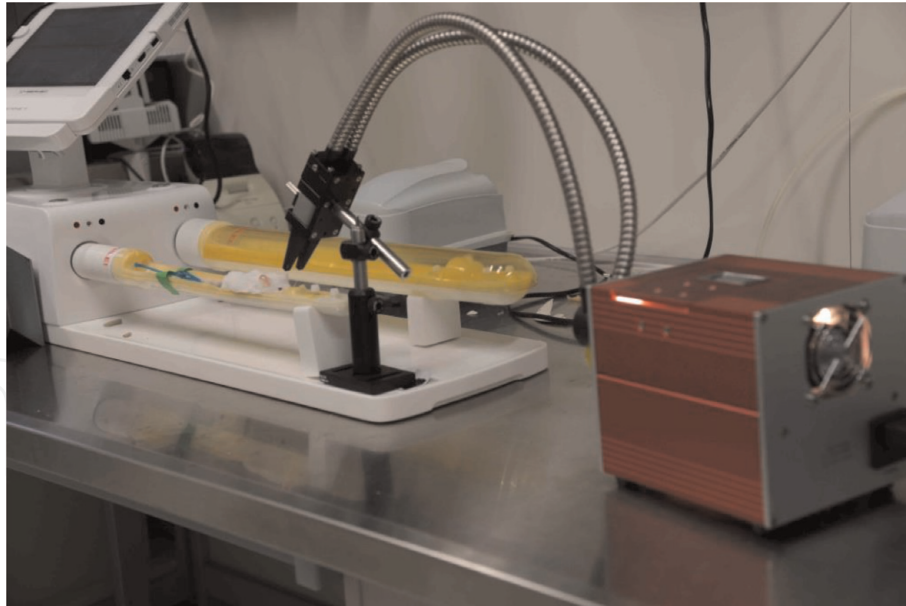


Figure 1. Shows the experimental setup with the Chromatoscope in close view of the mouse. The heart rate, respiration, and anesthetic airflow were monitored.

at 24°C (**Figure 1D**), There was free access to food and water. The vital signs including heart rate, respiration, and anesthetic airflow were monitored. All procedures were in compliance with the “Principles of laboratory animal care” (NIH publication no. 85e23, revised 1985) and were approved by the Institutional Animal Care and Use Committee in the state of Saxony, Germany as recommended by the responsible local animal ethics review board (Regierungspräsidium Leipzig, TVV08/13, Germany).

2.2 Statistical analysis

The results were presented as mean \pm SD and graphic plots show mean/SE/1.96*SE where applicable. We performed paired *t*-test statistics and one-way analysis of variance (ANOVA) for comparison of stimulus and dark conditions, for assessment of stimulus effects. Multivariate analysis of variance (MANOVA) with repeated measures was used where applicable. The latter was followed by planned *t*-tests to examine specific differences. The level of significance was at $p < 0.05$.

2.3 Fourier analysis

Prior to undertaking the time-series analysis, we examined the stationarity of the series by applying the Augmented Dickey-Fuller (ADF) test using the STATA (Stata Corp LLC, College Station, TX, USA) as described in detail elsewhere [20]. The ADF suggest that the time series data were strongly stationary without transformation. Fourier analysis was applied to examine the cyclical patterns of data of the mean \pm SD SUV values. It was presumed that the cyclical components may correlate to the frequency of neuronal discharges in a given region of the brain during the observed phenomenon. The analysis was to uncover a few recurring cycles of different lengths in the time series of metabolic activity that may reveal the random noise of neuronal activity. The software analyses were performed using Statistica for Windows (StatSoft, OK, USA) and SPSS Version 20 (IBM). The module for Fourier transform algorithm used is called the time-series and forecasting module (Statistica for Windows, StatSoft, OK, USA). The spectrum analysis was applied to the mean \pm SD SUV values provided in **Table 3**.

The Fourier analysis decomposed the original time series into components of sine and cosine functions at different frequencies, so as to reveal the important frequency region. The wavelength ν of a sine or cosine function is expressed as the number of cycles per unit time (*frequency*). The length of time required for one full cycle is denoted as the period T of a sine or cosine function, given by $T = 1/\nu$. The equation was restated as a linear multiple regression model, where the dependent variable is the observed time series, and the independent variables are the sine functions of all possible (discrete) frequencies. Thus the multiple regression model could be expressed as:

$$x_t = a_0 + \sum_{k=1}^q \quad (1)$$

The lambda (λ) notation is the frequency expressed in radians per unit time, given by $\lambda = 2\pi\nu$, where $\pi = 3.1416$. The degree of correlation with the data is represented as the regression coefficients for the cosine parameters a_k and sine parameters b_k . The different sine and cosine functions are denoted as q ; where there are $n/2 + 1$ cosine functions and $n/2 - 1$ sine functions. The series could be completely replicated from the underlying functions of many different sinusoidal waves as there are data points. For a sinusoidal function to be identified, there must be at least two data points of high peak and low trough. The Fourier algorithm requires that the length of the input series is equal to a power of 2 [24], if the number of data points in the series are odd, then the last data point is ignored or additional computations have to be performed. The Fourier algorithm identifies the correlation of sine and cosine functions at different frequencies in observed time-series data. When a large correlation is identified, this suggests strong periodicity of the respective frequencies in the data.

The Fourier time-series analysis of any periodic signal is a summation of mutually independent sine and cosine functions of orthogonal pair of matrices with one fundamental frequency and infinite number of harmonics. The periodogram is the summed squared coefficients at each frequency given by:

$$P_k = \text{sine coeff.}^2 + \text{cosine coeff.}^2 \quad n/2 \quad (2)$$

where P_k denotes the periodogram value at frequency ν_k and n is the overall length of the time series. Many chaotic periodogram spikes result from substantial random fluctuation of the periodogram values. Of practical importance are the plots at frequencies with the greatest spectral densities, which consists of many adjacent frequencies. These frequencies contribute most to the overall periodic behavior of the series. The smoothing of the periodogram values was made via a weighted moving average transformation. As described in detail elsewhere [20], we applied the Hamming window, which for each frequency, the weights for the weighted moving average of the periodogram values are computed as follows:

$$w_j = 0.54 + 0.46 * \cos (\pi * j/p) \quad (3)$$

(for $j = 0$ to p)

$$w_{-j} = w_j \quad (4)$$

(for $j \neq 0$)

The greatest weight functions to the observation being smoothed are assigned in the center of the window and increasingly smaller weights are given to values that are further away from the center. The periodogram values of “white noise” input series will result in an exponential distribution.

The time-series was obtained as 20 data points for each stimulus condition for male and female mice, respectively, as shown in **Table 2**. The software analysis begins in Fourier analysis dialog, by choosing spectral density estimates and the Hamming window. Then select *Plot* to display cyclical patterns in graphs for male and female mice, respectively. The single series Fourier analysis was used to derive spectral density estimates that were plotted, and the frequency regions with the highest estimates were marked as peaks. The peak (as maxima) was identified as the spectral density estimates between two minima, and was used to examine the effects of stimuli on cortical and subcortical sites, respectively. The spectral density peak identified as cortical (C-peak) occurred at 0.2 and subcortical (S-peaks) occurred at 0.4, respectively. The stimulus responses was evaluated using the area under the curve derived for a particular stimulus compared to that derived from another stimulus or baseline condition. The region included in the analysis comprised five data points from trough-to-peak-to-trough for the C-peak and S-peak, respectively, shown as Fourier spectral density coefficients in **Table 2**.

2.4 Preclinical PET-MR

Figure 1 shows the mouse on a special mouse bed in prone position, while heated up to 37°C. The head was affixed to a mouth piece for the anesthetic gas supply with isoflurane in 40% air and 60% oxygen (Anesthesia unit U-410, AgnTho’s AB, Sweden; Gas blender 100, MCQ Instruments, Italy). The respiration, gas flow, and anesthesia were monitored. The animals were injected intraperitoneal with about 15 MBq of [¹⁸F]FDG, followed by a PET-MR scan using a preclinical PET-MR Scanner (nanoScan®, Mediso Medical Imaging Systems, Hungary). For the image processing, the PET image were corrected for scatter, dead time, attenuation (AC), and random coincidences, based on a whole body (WB) MR scan. Image reconstruction parameters for the list mode data were 3D-ordered subset expectation maximization (OSEM), which included four iterations, six subsets, energy window: 400–600 keV, coincidence mode: 1–5, and ring difference 81.

The procedure involved that the PET data were collected by a continuous WB scan during the entire investigation. The latter was followed by a T1 weighted WB gradient echo sequence (GRE, TR = 20 ms; TE = 6.4 ms) performed for AC and anatomical orientation. The SUV is calculated by two ways: first pixel-wise yielding a parametric image and over a volume of interest (VOI). This procedure was followed for any image acquired at time point t , and for all images of a dynamic series acquired at multiple time points. The mean SUV is defined as the ratio of (1) the tissue radioactivity concentration c (e.g. in MBq/kg = kBq/g) at time point t and (2) the *injected activity* (e.g. in MBq, extrapolated to the same time t) divided by the *body weight* (e.g. in kg). PET studies were conducted on the same animals repeatedly on consecutive days without randomization to keep the daytime of measurement (e.g. the glucose/insulin levels) constant, considering the diurnal circadian rhythm. The weight was monitored and there was no significant change in weight of the animals over the several days of study in male and female mice (**Table 1**). The intraperitoneally injected radiotracer ([¹⁸F]FDG) dose in male and female mice did not vary significantly over the several days of the study (**Table 1**).

The measurements of male (10.1 ± 1.5 mmol/L) and female (7.8 ± 1.8 mmol/L) mice random blood sugar levels were similar. All animals were at the end of the study euthanized by cervical dislocation under anesthesia.

Experimental days	Body weight (g)		Dose of radiotracer i.p (MBq)	
	Male mice	Female mice	Male mice	Female mice
Day 1	34.5 ± 2.8	25.6 ± 1.7	12.05 ± 1.23	12.7 ± 1.23
Day 2	34.4 ± 2.4	25.4 ± 1.3	12 ± 0.9	12.7 ± 1.3
Day 3	33.7 ± 2.3	25.5 ± 1.5	11.7 ± 1.2	12.6 ± 0.9
Day 4	34.7 ± 2.3	25.6 ± 1.2	10.6 ± 0.5	13.9 ± 0.7
Day 5	34.3 ± 2.5	26.4 ± 1.4	12.1 ± 1.7	11.4 ± 0.9
Day 6	34.6 ± 2.5	26.2 ± 1.4	10.8 ± 1.2	12.3 ± 1.2
Day 7	34.1 ± 2.6	26.5 ± 1.3	11.9 ± 1	12 ± 1.4

Table 1.
 The body weight and dose of injected radiotracer in male and female mice during the study.

2.5 Light stimulation studies

Light stimulation was accomplished using a custom-made device comprising a double barrel tunnel placed around both eyes and the nose ridge to separate both visual fields. At the end, there is a white screen illuminated by a remote light source. There is a groove in the light path before the screen that allows insertion of filters into the right or left visual fields, respectively. We used a tungsten coil filament light source of a general service lamp (OSL2 High-Intensity Fiber Light Source, Thorlabs Inc., Newton, New Jersey, USA) ran at a constant 21 V and 150 W. The maximum light output of the bulb was 40,000 foot candles (430,000 lux) with power at tip of fiber at a maximum bulb intensity of 1.4 W/m². The color temperature was about 3200 K and approximately 20 lumens/watt. The anesthetized mice had both eyes open at all times. At onset before stimulation, the animal was positioned with both eyes open and fixed peeping through the double barrel tunnel connected to a light source behind the white screen.

The stimulations' duration was 20 minutes and included: (1) Dark in both eyes—the left and right eyes were covered with 5% dexpanthenol ointment (Bepanthen, Bayer, Germany); (2) Right monocular light (Light Rt_eye)—the right eye is open and fixed peeping through one open barrel connected to the light source, while the left eye is covered with ointment. (3). Left monocular light (Light Lt_eye)—the left eye is open and fixed peeping through one open barrel connected to the light source, while the right eye is covered with ointment. (4). Right monocular blue light (Blue Rt_eye)—the right eye is open and fixed peeping through one open barrel affixed with Deep Blue filter (No. 47B, short dominant wavelength (λ) of $S_\lambda = 452.7$ nm) connected to the light source, while the left eye is covered with ointment. (5). Left monocular blue light (Blue Lt_eye)—the left eye is open and fixed peeping through one open barrel affixed with Deep Blue Wratten filter (No. 47B, short dominant wavelength λ of $S_\lambda = 452.7$ nm) connected to the light source, while the right eye is covered with ointment. (6). Right monocular yellow light (Yellow Rt_eye)—the right eye is open and fixed peeping through one open barrel affixed with Deep Yellow Wratten filter (No. 12) connected to the light source, while the left eye is covered with ointment. (7). Left monocular yellow light (Yellow Lt_eye)—the left eye is open and fixed peeping through one open barrel affixed with Deep Yellow Wratten filter (No. 12) connected to the light source, while the right eye is covered with ointment.

2.6 Rationale for visual stimulation

Color stimulation was accomplished using opponent blue/yellow colors of optical homogenous filters placed in the light path of the animal Chromatoscope. The Kodak Wratten filters were Deep Blue (No. 47B) of short $S_\lambda = 452.7$ nm, Deep Yellow (No. 12) of medium $M_\lambda = 510.7$ nm, dominant wavelengths. The excitation purity and luminous transmittance for each filter were given in the manual (Kodak Photographic Filters Handbook (Publication No. B-3), Eastman Kodak Company, Rochester, New York, 1990). The color stimuli were designed to elicit responses from V1 ocular dominance columns. Most V1 neurons respond preferentially to inputs from one eye or the other. Human studies have shown that cells with common preference are organized into columns that alternate with columns of neurons with the opposite preference [8, 10, 11]. During monocular stimulations through one aperture of the double barrel, the other was closed to light reflected from the remote light source. Closure of the one aperture was used to maximize stimulation of the right or left visual pathways of the contralateral eye that projects to the area 17 and extrastriate visual cortex and also precludes binocular interaction due to stereopsis [8]. The dark condition was not a quiescent “resting state” but was rather considered a light stimulus-absent condition with non-photoc signal transduction of the “color Dark” through the visual pathways.

2.7 Data analysis

Measurements of SUV values were obtained over time for Group A (males) and Group B (females) under conditions of Dark, light, blue, yellow stimulations, for the whole brain, and in the right and left hemispheres, respectively. The registration and evaluation of the images were performed with ROVER (ABX advanced biochemical compounds, Radeberg, Germany, v.2.1.15) (**Figure 2A**). The anatomic orientation of the right and left hemispheres was performed using the MR information from the GRE scan. The PET/MR data were coregistered to delineate the volume of interest (VOI), and the data analysis was performed by two observers. The steps included: first, to manually coregister the PET images to the respective T1 weighted MR data of each animal. Then the next step was to identify using the MRI information from the GRE scan, the right and left hemispheres. We selected the VOI in a space stretching from the primary visual cortex to the extrastriate cortex. The region is perfused by both the ganglionic branches of lenticulostriate arteries and the cortical branches from the main stems of the MCA and PCA [6]. The VOI included a region in the visual cortex with radiotracer concentration in a sample

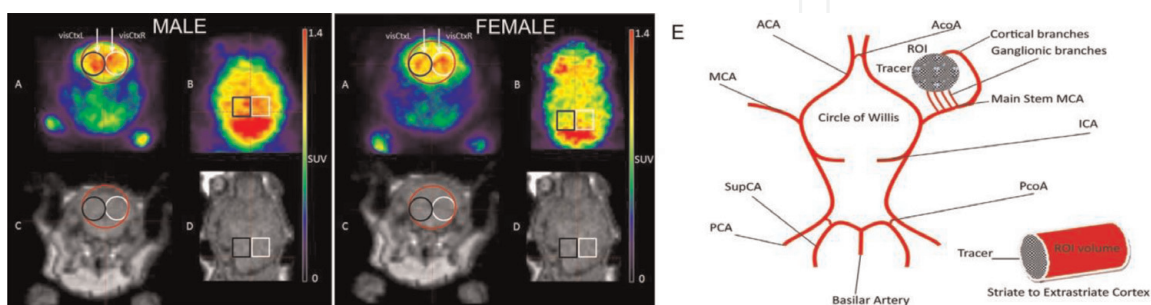


Figure 2.

The positioning of VOI on PET/MR images. The brain images of [18 F]FDG PET (A, B) and MR images (C, D) for male and female CD-1 mouse are shown in coronal (A, C) and transverse (B, D) sections. The color scale is displayed on the right side, and regions of highest SUV levels are shown in red. The MR T1 weighted images shown in coronal (C) and transverse (D) views were obtained by a gradient echo sequence with TE = 6.4 ms and TR = 20 ms. Figure 2E shows the distribution of ganglionic and cortical arteries in the ventral and dorsal streams as branches of the middle cerebral artery in the mouse brain.

volume of a cylindrical mask. The contour VOI is defined as a stack of planar, closed polygons called regions-of-interest (ROI) (**Figure 2A–F**), in male and female mice, respectively. The contours on the loaded images were outlined manually and semi-automatically to contain pixels within the contour boundaries for the VOI statistics. The contour vertices coordinates in triples (x, y, z) are defined as offsets are in [mm] in the x, y and z axes from the image origin. Further statistical analysis are performed in the two separated VOIs delineated (**Figure 2A–F**) which included two right and left sub-volumes (VOIs) with mask (x, y, z) pixel size (10, 10, 10) or (0.3, 0.3, 0.3 cm) placed in the visual cortex from the midpoint to the right border (visCtxR) and to the left border (visCtxL) of the midline.

3. Results

3.1 Experimental setup

Figure 1 shows the actual experimental setup for eye stimulation. The animals were placed in an animal cabinet with controlled day-light regimen, free access to water and food. The respiration and anesthetic gas flow were continually monitored during the experiment. The mice were placed in prone position on a special heated mouse pad with head affixed to a mouth piece. The eyes were fixed for 20 minutes light stimulation through the double barrel of the light source chromatoscope, described in detail elsewhere [5]. A whole body PET scan was started for a duration of 20 minutes using a preclinical scanner.

The distribution of ganglionic and cortical arteries in the ventral and dorsal streams as branches of the middle cerebral artery in the mouse brain is shown in **Figure 2E**.

The baseline condition was defined as Dark stimulus absent-condition in both eyes. The Dark condition could also elicit the perception of the “color Dark” and has been associated with changes in mCBFV indexed by transcranial Doppler [14].

We analyzed the mean \pm SD SUV data obtained in direct measurements (**Table 2**). We performed a MANOVA with repeated measures on the mean \pm SD SUV values, with a $7 \times 2 \times 2$ design: the stimulation of the visual cortex included seven levels of stimulations (both eyes Dark, right eye Light R, left eye Light L, right eye Blue R, left eye Blue L, right eye Yellow R, and left eye Yellow L), two levels of visual cortex (right visCtxR and left visCtxL), and two levels of gender (male and female). The mean \pm SD SUV was used as the dependent variables during stimulations. The F-statistics [20] for the observed main effect for stimulations was $F(6,228) = 7.621$, $MS = 0.356$, $p < 0.05$. The main effect for the visual cortex was $F(1,38) = 7.157$; $MS = 0.026$, $p < 0.05$. The gender main effect was $F(1,38) = 15.15$, $MS = 2.065$, $p < 0.05$. The observed interactions were stimulation \times gender: $F(6,228) = 6.405$, $MS = 0.299$, $p < 0.05$ and stimulations \times visual cortex $F(6,228) = 4.21$, $MS = 0.0141$, $p < 0.05$.

The Fourier spectral density coefficients obtained from the times series analysis of mean SUV are provided in **Table 3**. A MANOVA with repeated measures was performed with a $7 \times 2 \times 2 \times 2$ design. The dependent variables included seven levels of stimulations (Dark, Light R, Light L, Blue R, Blue L, Yellow R, and Yellow L), two levels of visual cortex (visCtxR and visCtxL), two levels of peaks (C-peak and S-peak), and two levels of gender (male and female). The results showed that the main effect for stimulations: $F(6,102) = 8.65$, $MS = 0.094$, $p < 0.05$. The main interactions were stimulations \times gender: $F(6,102) = 7.68$, $MS = 0.083$, $p < 0.05$, stimulations \times visual cortex \times gender: $F(6,102) = 3.4$, $MS = 0.00098$, $p < 0.05$, and stimulations \times visual cortex \times peaks: $F(6,102) = 3.4$, $MS = 0.00075$, $p < 0.05$.

Stimulation	Dark		LightR eye		LightL eye		BlueR eye		BlueL eye		YellowR eye		YellowL eye	
Visual cortex	visCtxR	visCtxL	visCtxR	visCtxL	visCtxR	visCtxL	visCtxR	visCtxL	visCtxR	visCtxL	visCtxR	visCtxL	visCtxR	visCtxL
Time	Male mice													
150	1.48	1.28	1.58	1.81	1.53	1.35	1.41	1.37	1.32	1.29	1.48	1.31	1.16	1.08
150	1.41	1.23	1.12	1.04	0.94	1.03	1.34	1.49	1.22	1.12	1.24	1.32	1.01	0.91
150	1.52	1.55	1.63	1.56	1.67	1.79	1.36	1.52	0.88	1.00	1.54	1.50	1.42	1.46
150	0.99	0.97	0.69	0.72	1.14	1.06	1.58	1.65	1.43	1.46	1.48	1.43	1.19	1.13
150	1.38	1.34	1.05	1.02	1.51	1.41	1.37	1.52	1.21	1.22	1.48	1.55	1.16	1.18
450	1.44	1.20	1.73	1.84	1.43	1.39	1.41	1.50	1.33	1.31	1.50	1.36	1.20	1.18
450	1.35	1.21	1.12	1.08	1.00	1.07	1.39	1.56	1.27	1.28	1.26	1.37	1.07	0.96
450	1.52	1.73	1.71	1.61	1.66	1.75	1.45	1.46	1.03	1.06	1.57	1.62	1.49	1.46
450	1.06	1.07	0.80	0.78	1.13	1.14	1.56	1.63	1.43	1.33	1.47	1.45	1.21	1.27
450	1.49	1.47	1.12	1.15	1.54	1.49	1.56	1.55	1.26	1.24	1.56	1.49	1.29	1.24
750	1.53	1.32	1.79	1.64	1.40	1.41	1.52	1.43	1.35	1.28	1.51	1.25	1.26	1.29
750	1.38	1.21	1.08	1.02	1.05	1.12	1.50	1.48	1.20	1.23	1.27	1.41	1.00	0.93
750	1.45	1.66	1.70	1.58	1.58	1.71	1.50	1.49	1.14	1.17	1.64	1.60	1.50	1.47
750	1.12	1.15	0.78	0.80	1.24	1.24	1.66	1.59	1.51	1.30	1.53	1.48	1.33	1.22
750	1.46	1.45	1.27	1.18	1.50	1.53	1.45	1.68	1.30	1.24	1.46	1.57	1.29	1.32
1050	1.48	1.41	1.70	1.74	1.40	1.33	1.46	1.47	1.40	1.30	1.60	1.38	1.30	1.26
1050	1.29	1.24	1.02	1.02	1.05	1.05	1.32	1.47	1.27	1.25	1.21	1.36	0.99	0.97
1050	1.55	1.61	1.74	1.63	1.62	1.55	1.41	1.49	1.22	1.18	1.57	1.59	1.50	1.50
1050	1.19	1.14	0.88	0.92	1.30	1.35	1.65	1.56	1.44	1.46	1.53	1.44	1.31	1.29
1050	1.44	1.37	1.24	1.30	1.54	1.49	1.48	1.68	1.28	1.25	1.52	1.46	1.40	1.43

Stimulation	Dark		LightR eye		LightL eye		BlueR eye		BlueL eye		YellowR eye		YellowL eye	
	visCtxR	visCtxL	visCtxR	visCtxL	visCtxR	visCtxL	visCtxR	visCtxL	visCtxR	visCtxL	visCtxR	visCtxL	visCtxR	visCtxL
Time	Female mice													
150	1.14	0.99	0.94	0.97	1.13	1.03	1.23	1.26	1.29	1.22	1.21	1.24	1.28	1.21
150	1.31	1.22	1.00	0.92	1.11	1.06	1.44	1.49	1.25	1.30	1.35	1.23	1.32	1.39
150	1.06	1.11	1.15	1.11	1.40	1.36	1.05	1.22	1.41	1.38	1.15	1.00	1.01	1.01
150	1.39	1.37	1.19	1.08	1.58	1.60	1.21	1.24	1.38	1.40	1.16	1.18	1.26	1.28
150	1.21	1.25	1.06	0.99	1.13	1.18	1.34	1.25	1.37	1.18	1.16	1.18	1.23	1.32
450	1.17	1.16	0.95	0.99	1.13	0.98	1.08	1.16	1.29	1.27	1.25	1.27	1.38	1.28
450	1.26	1.28	1.10	1.07	1.15	1.13	1.52	1.40	1.30	1.24	1.40	1.25	1.41	1.41
450	1.03	1.12	1.11	1.14	1.44	1.38	1.14	1.12	1.44	1.43	1.21	0.98	1.08	1.01
450	1.40	1.31	1.19	1.23	1.71	1.75	1.26	1.37	1.40	1.35	1.19	1.23	1.23	1.29
450	1.18	1.17	0.97	1.02	1.06	1.12	1.35	1.35	1.31	1.13	1.19	1.23	1.21	1.29
750	1.11	1.17	0.92	0.98	1.14	0.98	1.03	1.14	1.29	1.28	1.25	1.19	1.30	1.35
750	1.33	1.33	1.16	1.15	1.12	1.11	1.53	1.53	1.27	1.23	1.47	1.23	1.52	1.51
750	1.01	1.10	1.16	1.12	1.44	1.35	1.14	1.22	1.51	1.54	1.16	1.01	1.05	1.13
750	1.46	1.49	1.18	1.24	1.71	1.63	1.34	1.29	1.43	1.38	1.18	1.19	1.27	1.22
750	1.16	1.14	0.93	0.98	1.08	1.19	1.30	1.33	1.26	1.10	1.18	1.19	1.25	1.30
1050	1.17	1.05	0.91	0.98	1.04	1.01	1.04	1.05	1.34	1.34	1.27	1.20	1.28	1.25
1050	1.35	1.32	1.22	1.18	1.19	1.08	1.44	1.39	1.29	1.28	1.41	1.34	1.44	1.53
1050	0.97	1.09	1.13	1.06	1.43	1.39	1.14	1.11	1.44	1.39	1.23	1.08	1.14	1.09
1050	1.37	1.33	1.21	1.23	1.68	1.66	1.29	1.30	1.36	1.36	1.18	1.17	1.24	1.28
1050	1.11	1.14	0.92	0.88	1.03	1.11	1.39	1.35	1.20	1.12	1.18	1.17	1.24	1.20

Table 2. The standardized uptake values (SUV) for each time measurement obtained during dark condition, white light, blue, and yellow light stimulation in time series in each of the five male and female mice [20].

Stimulation	Dark		LightR eye		LightL eye		BlueR eye		BlueL eye		YellowR eye		YellowL eye	
	visCtxR	visCtxL	visCtxR	visCtxL	visCtxR	visCtxL	visCtxR	visCtxL	visCtxR	visCtxL	visCtxR	visCtxL	visCtxR	visCtxL
Male mice														
C-peak	0.005	0.006	0.012	0.014	0.002	0.003	0.014	0.004	0.001	0.002	0.002	0.005	0.002	0.005
	0.012	0.010	0.026	0.033	0.005	0.006	0.015	0.007	0.006	0.008	0.004	0.010	0.008	0.009
	0.038	0.023	0.105	0.141	0.014	0.023	0.021	0.016	0.029	0.022	0.019	0.025	0.033	0.038
	0.068	0.029	0.185	0.255	0.023	0.039	0.030	0.027	0.055	0.030	0.034	0.039	0.055	0.068
	0.043	0.015	0.103	0.148	0.013	0.021	0.017	0.017	0.037	0.016	0.019	0.023	0.031	0.038
S-peak	0.023	0.030	0.044	0.102	0.017	0.037	0.006	0.008	0.022	0.013	0.013	0.010	0.017	0.023
	0.081	0.162	0.170	0.485	0.095	0.224	0.014	0.011	0.061	0.039	0.051	0.021	0.073	0.098
	0.147	0.290	0.312	0.896	0.177	0.420	0.022	0.014	0.102	0.058	0.088	0.035	0.132	0.180
	0.080	0.157	0.169	0.490	0.101	0.239	0.013	0.011	0.058	0.030	0.048	0.020	0.073	0.100
	0.025	0.048	0.051	0.152	0.036	0.083	0.007	0.007	0.021	0.010	0.016	0.007	0.025	0.033
Female mice														
C-peak	0.002	0.010	0.002	0.010	0.003	0.006	0.003	0.009	0.004	0.002	0.002	0.001	0.003	0.006
	0.004	0.013	0.011	0.009	0.030	0.038	0.009	0.017	0.006	0.008	0.006	0.005	0.009	0.012
	0.007	0.017	0.049	0.025	0.193	0.233	0.014	0.012	0.019	0.037	0.028	0.017	0.034	0.033
	0.009	0.020	0.082	0.044	0.358	0.429	0.010	0.005	0.033	0.066	0.050	0.031	0.055	0.048
	0.005	0.012	0.046	0.025	0.197	0.234	0.006	0.003	0.020	0.038	0.027	0.020	0.030	0.025
S-peak	0.015	0.014	0.01	0.006	0.041	0.044	0.019	0.014	0.006	0.013	0.006	0.009	0.013	0.013
	0.086	0.054	0.009	0.012	0.061	0.034	0.1	0.064	0.009	0.023	0.012	0.022	0.042	0.055
	0.158	0.091	0.018	0.026	0.111	0.058	0.183	0.111	0.013	0.034	0.021	0.037	0.071	0.103
	0.087	0.049	0.016	0.029	0.064	0.035	0.102	0.06	0.008	0.019	0.012	0.02	0.039	0.059
	0.028	0.015	0.014	0.026	0.026	0.017	0.034	0.02	0.004	0.007	0.005	0.006	0.014	0.022

Table 3.

The Fourier spectral density coefficients obtained during Dark condition and stimulation with white, blue, and yellow lights through the right and left eye in male and female mice, respectively.

Stimulation visual cortex	Peaks	Mean ± Std. Dev.		Paired differences	95% CI of the difference		T-statistics		
		Paired stimuli		Paired mean Δ ± Std. Dev.	Lower	Upper	t	df	p
Male mice									
Right visual cortex									
		Dark	Light						
Dark vs. Light LvisCtxR	C-	0.033 ± 0.025	0.011 ± 0.008	0.022 ± 0.017	0.0006	0.043	2.851	4	0.05
	S-	0.071 ± 0.051	0.085 ± 0.063	-0.014 ± 0.013	-0.03	0.003	-2.251	4	NS
		Blue	Yellow						
Blue vs. Yellow LvisCtxR	C-	0.025 ± 0.022	0.026 ± 0.021	-0.0003 ± 0.004	-0.005	0.004	-0.197	4	NS
	S-	0.053 ± 0.033	0.064 ± 0.046	-0.011 ± 0.013	-0.027	0.005	-1.929	4	NS
Left visual cortex									
		Dark	Light						
Dark vs. Light RvisCtxL	C-	0.016 ± 0.009	0.118 ± 0.098	-0.101 ± 0.089	-0.212	0.009	-2.542	4	NS
	S-	0.137 ± 0.105	0.425 ± 0.32	-0.288 ± 0.214	-0.554	-0.021	-2.996	4	0.05
		Blue	Yellow						
Blue vs. Yellow RvisCtxL	C-	0.014 ± 0.009	0.02 ± 0.014	-0.006 ± 0.005	-0.012	-0.001	-3.011	4	0.05
	S-	0.01 ± 0.003	0.019 ± 0.011	0.009 ± 0.008	-0.019	0.001	-2.387	4	NS
Female mice									
Right visual cortex									
		Dark	Light						
Dark vs. White Light LvisCtxR	C-	0.005 ± 0.003	0.156 ± 0.144	-0.151 ± 0.142	-0.327	0.025	-2.382	4	NS
	S-	0.075 ± 0.057	0.061 ± 0.032	0.014 ± 0.028	-0.021	0.049	1.134	4	NS

Stimulation visual cortex	Peaks	Mean \pm Std. Dev.		Paired differences	95% CI of the difference		T-statistics		
		Paired stimuli		Paired mean $\Delta \pm$ Std. Dev.	Lower	Upper	t	df	p
		Blue	Yellow						
Blue vs. Yellow LvisCtxR	C-	0.017 \pm 0.012	0.026 \pm 0.02	-0.01 \pm 0.009	-0.021	0.002	-2.311	4	NS
	S-	0.008 \pm 0.003	0.036 \pm 0.024	-0.028 \pm 0.021	-0.054	-0.002	-3.017	4	0.05
Left visual cortex									
Dark vs. Light RvisCtxL	C-	0.015 \pm 0.004	0.023 \pm 0.014	-0.008 \pm 0.011	-0.022	0.006	-1.627	4	NS
	S-	0.045 \pm 0.032	0.02 \pm 0.01	0.025 \pm 0.029	-0.012	0.062	1.894	4	NS
Blue vs. Yellow RvisCtxL	C-	0.009 \pm 0.005	0.015 \pm 0.012	-0.006 \pm 0.012	-0.026	0.014	-0.822	4	NS
	S-	0.054 \pm 0.039	0.019 \pm 0.012	0.035 \pm 0.028	0.001	0.069	2.869	4	0.05

Table 4.

Paired samples statistics of Fourier coefficients during dark condition and stimulation with white light, blue, and yellow in male and female mice, respectively.

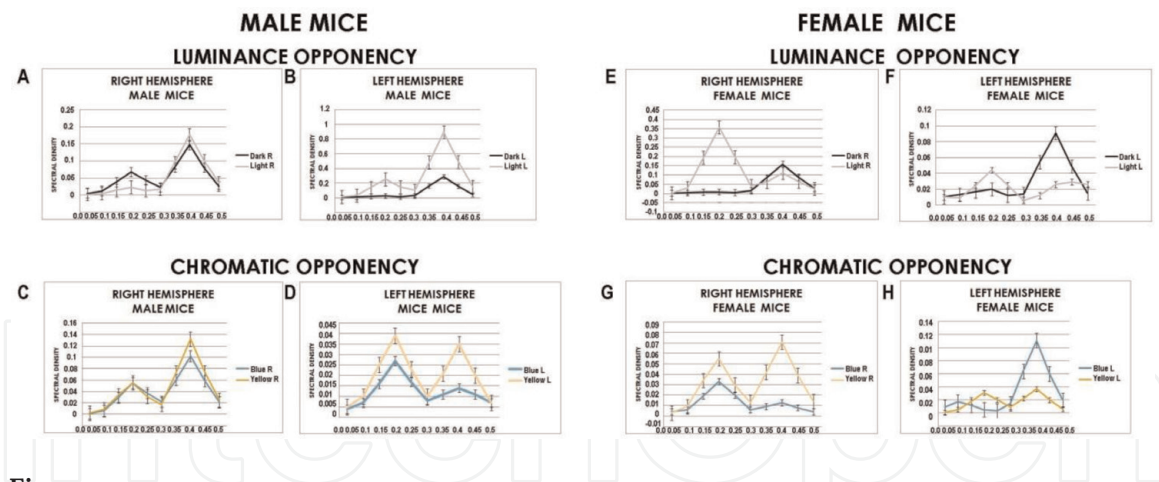


Figure 3.
 Spectral density plots of Fourier coefficients for male (A–D) and female mice, (E–H), respectively.

To examine luminance and chromatic opponency, paired t-test comparison was used and the results are summarized in **Table 4** and **Figure 3A–H**. In male mice, during dark versus light stimulation, the luminance opponency was accomplished by wavelength-differencing at S-peak by SLTP in the dorsal stream in the left visual cortex, $p < 0.05$ (**Figure 3B**). There was concurrent contralateral energy-encoding at C-peak in the ventral stream in the right visual cortex. There was concurrent energy-encoding occurred at the C-peak by CLTD in the ventral stream in the contralateral right visual cortex, $p < 0.05$ (**Figure 3A**). The chromatic opponency of blue versus yellow pairs, occurred by wavelength-differencing at cortical C-peak by CLTP in the ventral stream in the left visual cortex (**Figure 3D**).

In female mice, white light stimulation caused a resonance effect at C-peak in the ventral stream in the right visual cortex over a broad range of frequencies (**Figure 3E**), but not by luminance opponency response as seen in male mice, $p = \text{NS}$. Chromatic opponency by wavelength-differencing effects occurred at S-peak by SLTP in the dorsal stream in the right visual cortex, $p < 0.05$, (**Figure 3G**). Concurrently, there was a contralateral left hemisphere subcortical energy-encoding frequency-differencing at S-peak by SLTP within the dorsal stream in the left visual cortex, $p < 0.05$, (**Figure 3H**).

4. Discussion

4.1 Origins of spectral C-peak and S-peak

Fourier series could be applied to the periodic and quasi-periodic phenomena in the cerebrovascular system [15–20, 24–26]. Once the times series is proven to be stationary [20], as was in the present study, the two basic postulates for Fourier analysis namely, periodicity and linearity are usually satisfied for the oscillatory components of the cerebrovascular system [25, 26]. Specialized neurons processing the light stimuli would cause modulation of the frequency response to the stimuli, hence it is expected that there would be a change in the area under the spectral density curves at C-peak and S-peak compared to non-response or stimulus-absent condition. In the present study, as in previous studies [18, 20], the origin of C-peak and S-peak could be derived from the spectral analysis. The C-peak and S-peak occurred at multiples of the first harmonic, at the second and third harmonics, respectively. It has been demonstrated that, in the vascular system, the first five harmonics contain 90% of the pulsatile energy of the system [37]. The frequencies obtained in the spectral plots could be converted to cycles per second (Hz),

assuming that the fundamental frequency of cardiac oscillation was the mean heart rate in mice. In mice, the mean heart rate per second of CD-1 mice = 515 ± 30 bpm/60 seconds = 8.6 Hz as the fundamental frequency f of the first harmonic [38]. Hence, the reflection site for the fundamental frequency emanates from a distance at $D_1 = \frac{1}{4}\lambda$ or $c/4f$ or $1.91 \text{ m/s}/(4 \times 8.6 \text{ Hz}) = 0.055 \text{ m/s}$ or 5.5 cm, where $c = 1.91 \pm 0.44 \text{ m/s}$, is the wave propagation velocity [38]. The calculated distances only approximate the actual arterial lengths. If we account for vascular tortuosity, the estimated distance (5.5 cm) is from the terminal vessels in the brain to an imaginary site of summed reflections at the aorto-iliac junction in the mice. The reflection site for the C-peak which occurred at the second harmonic, could be estimated to originate from an arterial length given by $D_2 = 1/8\lambda$ or $c/8 \times 2f$, or $1.91 \text{ m/s}/(8 \times (2 \times 8.6 \text{ Hz or } 17.2 \text{ Hz})) = 0.0139 \text{ m}$ or 1.4 cm. The latter arterial length approximates the visible length from the main stem of the major cortical arteries around the cerebral convexity to the end occipitotemporal junction as shown in mouse brain (**Figure 2**). Similarly, we can estimate the origin of the S-peak which occurred at the third harmonic, at a distance given by $D_3 = 1/16\lambda$ or $c/16 \times 3f$, or $1.91 \text{ m/s}/(16 \times (3 \times 8.6 \text{ Hz or } 25.8 \text{ Hz})) = 0.0046 \text{ m}$ or 0.46 cm or 4.6 mm. The latter arterial length approximates the visible length from the main stem of the major cortical arteries to the distal arterioles of the ganglionic branches [6]. The derived frequencies also correspond to known electrical activity in the brain [39], for example, the cortical frequency of 17 Hz is within the beta rhythm range ($\sim 14\text{--}18$ Hz) which is implicated in cortical areas of higher visual hierarchy in top-down feed-back processing in the visual system [39]. This may suggest that, beta rhythms could predominate in cortico-subcortical patterns of activation in male mice. On the other hand, in female mice, 25 Hz is the frequency of the rhythm of gamma waves [40] implicated in the subcortico-cortical circuits during visual processing. The ratio of the length of the ganglionic branches to the cortical branches is 1:3 in mice, this same ratio is found in human subjects [18, 19]. This may suggest that the cerebral vaso-architecture was optimized in mammals to facilitate vascular harmonic oscillations with matched frequency of neuronal activity within the brain.

4.2 Gender differences in asymmetry for color processing and memory formation

Memory processing in mice has been fairly well studied, particularly the left-right dissociation [41]. It has been shown that silencing CA3 area of the left hippocampus impaired associative spatial long-term memory, whereas the equivalent manipulation in the right hippocampus did not [41]. In the present study, in male mice, chromatic opponency of yellow/blue pair was associated with significant differentiation of CLTP processes at cortical C-peaks, which may suggest that the wavelength-differencing of color and its associative memory processes were integrated within the same cortical-subcortical circuits in the left hemisphere. On the other hand, in female mice, the chromatic opponency involved significant differentiation at S-peak by SLTP for yellow from blue by SLTD (**Figure 3G**). This would imply that, the associative color memory processes would require contralateral left hemisphere retrieval from subcortical memory circuits. Hence, in female mice, we observed significant right visual cortex wavelength-differencing by SLTP concurrently with left visual cortex energy-encoding frequency-differencing of blue by SLTP processes (**Figure 3H**). In other words, in male mice, color processing and associated memory retrieval implicated ipsilateral cortico-subcortical circuits in the left visual cortex. In contrast, in female mice, color processing occurred in the right visual cortex, while associated memory retrieval involved contralateral left visual cortex through right-to-left transcallosal subcortical circuits.

There are important features, LTP and LTD models, that characterize synaptic and cellular events that may underlie memory formation. LTP model exhibits numerous properties expected of a synaptic associative memory mechanism, such as rapid induction, associative interactions, persistence, synapse specificity, and dependence on correlated synaptic activity. The changes in LTP and LTD would alter the frequency domain, hence, Fourier time-series analysis could provide useful insights into the mechanistic strategies employed in memory processing. The mechanisms underlying long-term potentiation and long-term depression could be deduced from what is known. The main excitatory neurotransmitter in the brain is glutamate. The role of glutamate in the processes that induce potentiation have not been fully elucidated. However, it has been suggested that the mechanism by which LTP is induced does not involve AMPA (alpha amino-3-hydroxy-5-methylisoxazole-4-propionic acid) receptors, but the synaptic response of potentiation implicates AMPA receptor activity [28, 29, 42]. The latter processes critical for LTP development begins with sufficient depolarization of the cell membrane containing the NMDA (N-methyl-D-aspartate) channels, that cause Mg^{2+} to leave the channels, and glutamate activation of the NMDA receptors opens the channels, allowing Ca^{2+} to rush into the neuron [28, 29, 42]. On the other hand, in the subcortical region, a counter trend develops due to combined activation of other receptors such as the metabotropic receptor, which results in a paradoxical long-lasting decrease in the responsiveness of the AMPA receptors to glutamate release [28, 29, 42]. Although, these cellular processes cannot be tracked *in vivo*, there is now the prospect of using this new imaging approach (*f*PETS/MRI) to study LTP and LTD in the ventral and dorsal streams, respectively. It is hoped that, this may offer insight into processes within the cortico-subcortical neural networks, which may correlate with findings from cellular studies of deep structures in the dorsal striatum, accumbens, and prefrontal cortex following stimulation of fornix-fimbria bundle [28, 29, 42, 43]. Moreover, it has been suggested that gamma-amino-butyric acid (GABA) modulates the color-opponent bipolar cells either through activating GABA receptors on these cells directly or those on cone terminals indirectly [44].

4.3 Resolving the binding problem

The findings in this chapter suggest that a hypothesis for the binding problem could be postulated. The first binding problem involving segregation of the different colors (up to 10 million) [45] occurs by generation of continuous highly dynamic variation of cortical long-term potentiation when modulated by inputs from wavelength-sensitive retinal S-cones through retino-geniculate-cortical pathways to specialized cortical neuronal cells in the ventral stream in male mice. For the second binding problem, in male mice, there is ipsilateral left hemisphere color memory combinatorial computation. On the other hand, in female mice, the process of segregation of colors occurred by subcortical long-term potentiation in the dorsal stream in the right visual cortex. The second binding problem of combinatorial computation occurred through synchronous activation by subcortical long-term potentiation and frequency differencing in the left visual cortex. In male mice, there is a distinct spatial separation of luminance and chromatic signal processing in different orthogonal axes (**Figure 3B**), with subcortico-cortical luminance axis, and an orthogonal cortico-subcortical chromatic axis (**Figure 3D**), within the same ipsilateral color space. On the other hand, in female mice, the color space appears different, where luminance is completely independent outside the color space. The chromatic axis for wavelength-differencing in the right visual cortex (**Figure 3G**) runs in opposite direction to the chromatic axis for frequency-differencing in the left visual cortex (**Figure 3H**), in female mice. Similar observations of

reversed color space in female subjects compared to males have been made in human studies [17].

In conclusion, Fourier time-series analysis was helpful to improve both spatial and temporal resolution of *f*PET/MRI for study of color processing in the visual system. Spatial resolution and temporal sequence underlies the perceptive and memory processes. The present study demonstrated gender differential responses to light and color stimuli that confirm the proposed light hypothesis for cerebral asymmetry which posits that, there is a phenotypic neuroadaptation to the environmental physical constraints of light, which leads to phenotypic evolution and genetic variation of X-Y gene pairs that determined hemispheric asymmetry. The main aim of the evolutionary trend is to optimize perception of the “whole” environment by functional coupling of the genes for complementarity of brain hemispheres within self, and between genders [16, 17]. There is potential for use of these findings in animal models of memory deficits in brain degenerative diseases. The application to the binding problem needs further exploration, moreover, it has been proposed that the spatio-temporal synchronization of the iterative processes culminate in phenomenal awareness [46]. The present work, by demonstrating the potential of *f*PETS as a computational approach for studying the effects of color processing of conscious experience, has a wide range of applications in several areas including in neuroscience and artificial intelligence.

Competing interests

The authors declare no competing financial or non-financial interests.

Author contributions

P.C.N. and P.B. designed the concept of the studies. P.C.N. and M.K. acquired and analyzed the PET/MRI data in mice. P.C.N. performed the Fourier analysis. P.C.N., M.K., and P.B. participated in writing the paper.

Author details


Philip C. Njemanze^{1*}, Mathias Kranz² and Peter Brust²

¹ Neurocybernetic Flow Laboratory, Chidicon Medical Center, International Institutes of Advanced Research Training, Owerri, Imo State, Nigeria

² Helmholtz-Zentrum Dresden—Rossendorf, Department of Neuroradiopharmaceuticals, Research Site Leipzig, Institute of Radiopharmaceutical Cancer Research, Germany

*Address all correspondence to: philip.njemanze@chidicon.com

IntechOpen

© 2019 The Author(s). Licensee IntechOpen. This chapter is distributed under the terms of the Creative Commons Attribution License (<http://creativecommons.org/licenses/by/3.0>), which permits unrestricted use, distribution, and reproduction in any medium, provided the original work is properly cited. 

References

- [1] Ungerleider LG, Haxby JV. 'What' and 'where' in the human brain. *Current Opinion in Neurobiology*. 1994;4:157-165
- [2] Ungerleider LG, Mishkin M. Two cortical visual systems. In: Goodale MA, Mansfield RJQ, editors. *Analysis of Visual Behavior*. Cambridge: MIT; 1982. pp. 549-586
- [3] Perry CJ, Fallah M. Feature integration and object representations along the dorsal stream visual hierarchy. *Frontiers in Computational Neuroscience*. 2014;8:84
- [4] McKeefry DJ, Zeki S. The position and topography of the human colour centre as revealed by functional magnetic resonance imaging. *Brain*. 1997;120(Pt 12):2229-2242
- [5] Njemanze PC, Kranz A, Amend M, Hauser J, Wehrli BP. Gender differences in cerebral metabolism for color processing in mice: A PET/MRI Study. *PLoS One*. 2017;12:e0179919
- [6] Gray H, Clemente CD. *Gray's Anatomy of the Human Body*, 30th American edition. Philadelphia: Lippincott Williams & Wilkins; 1984
- [7] Takechi H, Onoe H, Shizuno H, Yoshikawa E, Sadato N, Tsukada HY, et al. Mapping of cortical areas involved in color vision in non-human primates. *Neuroscience Letters*. 1997;230:17-20. DOI: 10.1016/S0304-3940(97)00461-8
- [8] Gouras P. *The Perception of Color: Vision and Dysfunction*. England: Macmillan; 1991. pp. 179-197
- [9] Daw NW. Goldfish retina: organization for simultaneous color contrast. *Science*. 1967;158:942-944
- [10] Livingstone MS, Hubel DH. Anatomy and physiology of a color system in the primate visual cortex. *The Journal of Neuroscience*. 1984;4:309-356
- [11] Kraft JM, Brainard DH. Mechanisms of color constancy under nearly natural viewing. *Proceedings of the National Academy of Sciences of the United States of America*. 1999;96:307-312
- [12] Conway BR. Spatial structure of cone inputs to color cells in alert macaque primary visual cortex (V-1). *The Journal of Neuroscience*. 2001;21:2768-2783
- [13] Zeki S. *A Vision of the Brain*, Plate 16. Cambridge MA: Blackwell Scientific; 1993
- [14] Njemanze PC, Gomez CR, Horenstein S. Cerebral lateralization and color perception: A transcranial Doppler study. *Cortex*. 1992;28:69-75
- [15] Njemanze PC. Asymmetric neuroplasticity of color processing during head down rest: A functional transcranial Doppler spectroscopy study. *The Journal of Physiology*. 2008;15:49-59
- [16] Njemanze PC. Gender-related asymmetric brain vasomotor response to color stimulation: A functional transcranial Doppler spectroscopy study. *Experimental & Translational Stroke Medicine*. 2010;2:21
- [17] Njemanze PC. Gender-related differences in physiologic color space: A functional transcranial Doppler (fTCD) study. *Experimental & Translational Stroke Medicine*. 2011;3(1)
- [18] Njemanze PC. Cerebral lateralisation for facial processing: Gender-related cognitive styles determined using Fourier analysis of mean cerebral blood flow velocity in the middle cerebral arteries. *Laterality*. 2007;12:31-49

- [19] Njemanze PC. A new functional transcranial Doppler spectroscopy (fTCDs) study of cerebral asymmetry during neurocognitive functions in men and women. In: Gunarathne G, editor. *Advancements and breakthroughs in ultrasound imaging*. Rijeka: InTech; 2013. pp. 137-166
- [20] Njemanze PC, Kranz M, Brust P. Fourier analysis of cerebral metabolism of glucose: Gender differences in mechanisms of color processing in the ventral and dorsal streams in mice. *Forecast*. 2018;**1**:135-156. DOI: 10.3390/forecast1010010
- [21] Yarowsky PJ, Ingvar DH. Symposium summary. Neuronal activity and energy metabolism. *Federation Proceedings*. 1981;**40**:2353-2362
- [22] Fox PT, Raichle ME. Focal physiological uncoupling of cerebral blood flow and oxidative metabolism during somatosensory stimulation in human subjects. *Proceedings of the National Academy of Sciences of the United States of America*. 1986;**83**: 1140-1144
- [23] Dahl A, Lindegaard K-F, Russell D, Nyberg-Hansen R, Rootwelt K, Sorteberg W, et al. A comparison of transcranial Doppler and cerebral blood flow studies to assess cerebral vasoreactivity. *Stroke*. 1992;**23**:15-19
- [24] Bloomfield P. *Fourier Analysis of Time Series: An Introduction*. New York: Wiley; 1976
- [25] Attinger EO, Anne A, McDonald DA. Use of Fourier series for analysis of biological systems. *Biophysical Journal*. 1966;**6**:291-304
- [26] Njemanze PC, Beck OJ, Gomez CR, Horenstein S. Fourier analysis of the cerebrovascular system. *Stroke*. 1991;**22**: 721-726
- [27] Schuett S, Bonhoeffer T, Hübener M. Mapping retinotopic structure in mouse visual cortex with optical imaging. *The Journal of Neuroscience*. 2002;**22**:6549-6559
- [28] Bliss TV, Lomo T. Long-lasting potentiation of synaptic transmission in the dentate area of the anaesthetized rabbit following stimulation of the perforant path. *The Journal of Physiology*. 1973;**232**:331-356
- [29] Ito M. Long-term depression. *Annual Review of Neuroscience*. 1989; **12**:85-102
- [30] Xie X, Barrionuevo G, Berger TW. Differential expression of short-term potentiation by AMPA and NMDA receptors in dentate gyrus. *Learning & Memory*. 1996;**3**:115-123
- [31] Escobar ML, Derrick B. Long-term potentiation and depression as putative mechanisms for memory formation. In: Bermudez-Rattoni F, editor. *Neural Plasticity and Memory: From Genes to Brain Imaging*. Boca Raton (FL): CRC Press; 2007
- [32] Kang HS, Han MH, Kwon BJ, Kwon OK, Kim SH, Chang KH. Evaluation of the lenticulostriate arteries with rotational angiography and 3D reconstruction. *American Journal of Neuroradiology*. 2005;**26**:306-312
- [33] Campbell KB, Lee LC, Frasch HF, Noordergraaf A. Pulse reflection sites and effective length of the arterial system. *The American Journal of Physiology*. 1989;**256**:H1684-H1689
- [34] Hutcheon B, Yarom Y. Resonance, oscillation and the intrinsic frequency preferences of neurons. *Trends in Neurosciences*. 2000;**23**:216-222
- [35] Revonsuo A, Newman J. Binding and consciousness. *Consciousness and Cognition*. 1999;**8**:123-127. DOI: 10.1006/ccog.1999.0393. PMID 10447994

- [36] Smythies JR. *The Walls of Plato's Cave: The Science and Philosophy of Brain, Consciousness and Perception*. Aldershot; Brookfield, USA: Avebury. ISBN: 978-1-85628-882-8. OCLC 30156912
- [37] McDonald DA. *Blood Flow in Arteries*. Vol. 1974. Baltimore: Williams & Wilkins Co. pp. 311-350
- [38] Di Lascio N, Stea F, Kusmic C, Sicari R, Faita F. Non-invasive assessment of pulse wave velocity in mice by means of ultrasound images. *Atherosclerosis*. 2014;**237**:31-37. DOI: 10.1016/j.atherosclerosis.2014.08.033
- [39] Bastos AM et al. Visual areas exert feedforward and feedback influences through distinct frequency channels. *Neuron*. 2015;**85**:390-401
- [40] Fries P. Neuronal gamma-band synchronization as a fundamental process in cortical computation. *Annual Review of Neuroscience*. 2009;**32**: 209-224
- [41] Shipton OA, El-Gaby M, Apergis-Schoute J, Deisseroth K, Bannerman DM, Paulsen O, et al. Left-right dissociation of hippocampal memory processes in mice. *PNAS*. 2014;**111**: 15238-15243. DOI: 10.1073/pnas.1405648111
- [42] Clapp WC, Eckert MJ, Teyler TJ, Abraham WC. Rapid visual stimulation induces N-methyl-D-aspartate receptor-dependent sensory long-term potentiation in the rat cortex. *Neuroreport*. 2006;**17**:511-515
- [43] Jiang B, Akaneya Y, Hata Y, Tsumoto T. Long-term depression is not induced by low-frequency stimulation in rat visual cortex in vivo: A possible preventing role of endogenous brain-derived neurotrophic factor. *The Journal of Neuroscience*. 2003;**23**: 3761-3770
- [44] Zhang DQ, Yang X. GABA modulates color opponent bipolar cells in carp retina. *Brain Research*. 1998;**792**: 319-323
- [45] Frisén L. *Clinical Tests of Vision*. New York: Raven Press; 1990
- [46] Singer W. Consciousness and the binding problem. In: Marijuán PC, editor. *Cajal and Consciousness: Scientific Approaches to Consciousness on the Centennial of Ramón y Cajal's Textura*. New York, NY: The New York Academy of Sciences; 2001. pp. 123-146